Research Letter **DOI:** 10.15541/jim20230549

First-principles Investigation of Single 3d Transition Metals Doping Graphene Vacancies for CO_2 Electroreduction

JIN Yuxiang[1], SONG Erhong[2], ZHU Yongfu[1]

(1. School of Materials Science and Engineering, Jilin University, Changchun 130025, China; 2. Shanghai Institute of Ceramics, Chinese Academy of Sciences, Shanghai 200050, China)

Abstract: Among all options of carbon neutrality, conversion of CO_2 into valuable chemicals by electrocatalytic reduction exhibit outstanding performance. However, due to the numerous products and complex pathways of CO_2 electrocatalytic reduction, the exact factors affecting the activity of CO_2 electrocatalytic reduction have not yet been identified. In addition, the CO_2 electrocatalytic reduction process is often accompanied by hydrogen evolution reaction (HER). Therefore, it is still challenging to design a catalyst with high selectivity and high activity for specific product. Herein, this study systematically investigated the potential of 3d transition metal-based single-atom catalysts (SACs) positioned at graphene single vacancies (TM@C_{SV}), as well as double vacancies (TM@C_{DV}), for the CO_2 reduction reaction (CO_2RR) using first-principles. The exploration encompassed substrate stability, CO_2 adsorption, and the HER as the main competing reaction. Through the careful screening of 20 catalysts formed by Sc, Ti, V, Cr, Mn, Fe, Co, Ni, Cu and Zn doped graphene defects, several promising catalysts were identified: Sc@C_{SV} situated on graphene single vacancies, Sc@C_{DV} and Ti@C_{DV} situated on graphene double vacancies. They could not only effectively adsorb CO_2 molecules, but also inhibit HER, the main competing reaction. In assessing their performance in CO_2RR, all exhibited selectivity toward HCOOH. Notably, Sc@C_{DV} demonstrated the best selectivity, requiring the lowest ΔG (0.96 eV) for efficient CO_2 conversion to HCOOH. Electronic structure analysis revealed that Sc@C_{DV} outperforms due to its optimal balance between ΔG of hydrogenation and the product desorption achieved through a moderate number of active electrons.

Key words: first-principle; single-atom catalyst; CO_2 reduction reaction; HCOOH; carbon neutrality

Previous reliance on fossil fuels has resulted in significant CO_2 emissions, contributing to a range of environment issues[1-3]. In the pursuit of carbon neutrality, the catalytic reduction of CO_2 has garnered considerable attention[3-8]. CO_2 catalytic reduction encompasses both electrocatalytic and photocatalytic methods[9-12]. Electrochemistry, due to its adjustable reaction conditions and environmental friendliness, has been extensively studied for H_2, O_2, and N_2 reduction[13-22]. Likewise, CO_2 electrocatalytic reaction (CO_2RR) has been a subject attracting intense research. The products of CO_2RR include C1 products and multi-carbon products, such as CO, HCOOH, CH_3OH, CH_4, C_2H_4, and CH_3CH_2OH[23-27]. Electrocatalytic CO_2 reduction contributes to not only carbon neutrality but also economically valuable products. However, challenges like poor selectivity, high overpotentials, and low conversion efficiencies persist in CO_2RR research. Hence, identifying efficient electrocatalysts for CO_2RR is of paramount importance.

In a groundbreaking study, Qiao *et al*.[28] firstly introduced the concept of single-atom catalysts, achieving high activity for CO oxidation by preparing single-atom Pt catalysts with isolated Pt anchored on the surface of iron oxide nanocrystals. Since then, single-atom catalysts have garnered widespread attention due to their outstanding catalytic performance and high atom utilization[29-36]. The anchoring of single atom in two-dimensional (2D) materials presents a highly promising approach for catalyst design. For instance, Du *et al*.[37] effectively triggered the surface-mediated reaction of

Received date: 2023-11-30; **Revised date:** 2024-02-06; **Published online:** 2024-03-05
Foundation item: Science and Technology Commission of Shanghai Municipality (21ZR1472900, 22ZR1471600)
Biography: JIN Yuxiang (1999–), male, Master candidate. E-mail: jinyx21@mails.jlu.edu.cn
靳宇翔(1999–), 男, 硕士研究生. E-mail: jinyx21@mails.jlu.edu.cn
Corresponding author: ZHU Yongfu, professor. E-mail: yfzhu@jlu.edu.cn; SONG Erhong, associate professor. E-mail: ehsong@mail.sic.ac.cn
朱永福, 教授. E-mail: yfzhu@jlu.edu.cn; 宋二红, 副研究员. E-mail: ehsong@mail.sic.ac.cn

LiS_x by dispersing Co atoms in N-doped graphene, which is the primary material in batteries. They found out that the Co-N-C coordination as a center promoted the decomposition and travel of Li_2S during charging and discharging. Such catalysts also demonstrated significant potential in the study of CO_2RR. Hu *et al*.[38] developed an ultra-highly active Fe^{3+}-N-C single-atom catalyst that efficiently reduced CO_2 to CO at low potential. They identified isolated Fe^{3+} as active site by XAS analysis. Zhang *et al*.[39] anchored Ga to the nitrogen carbide surface, tuning the electronic structure of the central Ga atom through P and S atoms coordination. This led to the achievement of a low-overpotential CO production with an ultra-high Faradaic efficiency of 92%, surpassing other bulk Ga catalysts significantly. 2D planar-constructed single-atom catalysts, especially those on graphene, showed immense potential in CO_2RR. Graphene, a monolayer two-dimensional honeycomb structure composed of tightly connected carbon atoms[40-42], possesses excellent electrical and optical properties in materials science, energy, and biomedicine fields[43-46]. The establishment of stable single-atom catalysts on graphene surfaces holds promise for economically viable CO_2RR.

Metallic materials draw attention in the field of catalysis due to abundant active sites and better structural stability, but the economics of precious metals among them greatly limits the industrialization of catalysts, while 3d transition metals with abundant reserves are more inexpensive in comparison. Previous studies have pointed out that Cu of 3d transition metal is able to reduce CO_2 to hydrocarbons during CO_2RR[47-50]. However, the variety of active sites on the surface of pure metals makes it difficult to achieve high selectivity for specific products, and the fact that active sites all on the surface result in a waste of metal atoms inside. Therefore, metals are often modified to achieve better performance. For example, Reske *et al*.[51] demonstrated that nano-Cu displays better catalytic performance than bulk Cu by comparing Cu particles of different sizes. In addition, Jiang *et al*.[52] combined 3d transition metals with carbon-based materials to synthesize a series of M–N–C (M = Fe, Ni, Co, and Cu), of which Ni–N–C showed excellent catalytic performance for CO.

This study systematically explored 20 single-atom catalysts formed by doping 3d transition metals (Sc, Ti, V, Cr, Mn, Fe, Co, Ni, Cu, and Zn) in graphene defects, aiming to elucidate the potential of 3d transition metal doping upon graphene defects for CO_2RR. Initially, we examined their structures at single and double vacancies on the graphene surface and assessed the stability of $Sc@C_{DV}$ at room temperature through both thermodynamic and molecular dynamics analyses. Based on the screening of CO_2 adsorption ability and hydrogen evolution reaction (HER) inhibition ability, three catalysts, $Sc@C_{SV}$, $Sc@C_{DV}$ and $Ti@C_{DV}$ were identified. The potentials of $Sc@C_{SV}$, $Sc@C_{DV}$, and $Ti@C_{DV}$ were modeled to generate the $2e^-$ product by first-principles calculation. In contrast to the general CO_2RR theoretical studies, we expect to obtain efficient catalysts with excellent selectivity and activity through a series of systematic screenings, which is significant for achieving large-scale production. We explored the structure of TM@C and the CO_2RR performance of efficient catalysts based on the first-principles calculation. The stability of $Sc@C_{DV}$ was analyzed based on electronic structure and molecular dynamics. Finally, we deeply explored the key factors affecting the CO_2RR activity in the perspective of electronic structure.

1 Computational methods

All density functional theory (DFT) calculations were performed using the Vienna *ab initio* Simulation Package (VASP)[53-54]. The exchange correlation function was treated by the generalized gradient approximation (GGA) of Perdew-Burke-Ernzerhof (PBE)[55]. The interaction between the valence electrons and ionic cores was described by the projector augmented wave (PAW) method[56-57]. The van der Waals force interactions were described using the DFT-D3 method[58]. All systems were spin-polarised. 4×4 graphene supercells were used as models. And a vacuum layer of 15 Å was created to avoid interactions arising from periodicity, as shown in Fig. S1. A 4×4×1 gamma grid was used for structural optimization. A 12×12×1 gamma grid was used for calculating the density of states (DOS). The plane wave truncation energy was set to 450 eV. The energy and force change convergence criteria were set to 1.0×10^{-7} eV and 0.02 eV/Å in all calculations, respectively.

The reaction free energy (ΔG) was determined by the CHE model suggested by Nørskov *et al*.[59]. The ΔG/eV without extra potential (U/V) was given by Eq. (1).

$$\Delta G = \Delta E + \Delta E_{ZPE} - T\Delta S \quad (1)$$

where ΔE/eV is the reaction energy, ΔE_{ZPE}/eV is the change of zero-point energy, T/K is the temperature, and ΔS/(J·mol^{-1}·K^{-1}) is the change of entropy.

The binding energy (E_b/eV) and formation energy (E_f/eV) were calculated respectively by Eq. (2, 3).

$$E_b = E_{total} - E^* - E_{substance} \quad (2)$$

$$E_f = E_{total} - E^* - E_{adsorbate} \quad (3)$$

where E_{total}/eV is the total energy of the system, E^*/eV is the energy of the free catalyst, $E_{substance}$/eV is the energy of the binding substance, and $E_{adsorbate}$/eV is the energy of the adsorption intermediate.

2 Results and discussion

2.1 Structure of TM@C

The binding affinity of transition metals (TM) to graphene surface vacancies was initially investigated. Previously, Li *et al*.[60] synthesized Ni single-atom catalysts (Ni@C) utilizing graphene double vacancies, showcasing the feasibility of constructing single-atom catalysts based on graphene vacancies. The structures of 3d metals binding to graphene single vacancies (SV) and double vacancies (DV), are presented in Fig. S1 and Fig. S2, respectively. All systems exhibit the formation of TM@C structures, and their formation energies are illustrated in Fig. S3. Notably, the formation energies for most of the TM@C are in the range from 5 to 8 eV, but only Zn@C_{SV}, Zn@C_{DV} and Cu@C_{SV} have formation energies of 1.27, 3.26 and 3.87 eV, respectively, which are significantly lower than those of the other TM@C. Thus, Zn@C_{SV}, Zn@C_{DV} and Cu@C_{SV} are less stable compared to other TM@C. Here Sc@C_{DV} is taken as a probe to investigate the structure as well as the charge density difference of TM-doped graphene defects, displayed in Fig. 1(a, b). In Sc@C_{DV}, Sc is coordinated to four adjacent carbon atoms, with the longest Sc–C bond measured as 2.24 Å. The bond lengths of the other coordination bonds are detailed in Table S1 and Table S2. The differential charge density plot illustrates substantial electron exchange between Sc and the surrounding C atoms, resulting in electron accumulation between Sc and C. Bader charge analysis indicates that the Sc atom bound at the double vacancy carries a charge of +1.32, and the Bader charge numbers of the other atoms are demonstrated in Table S1 and Table S2. In Fig. 1(c) the projected densities of states (PDOS) diagram of Sc@C_{DV} is depicted, revealing an overlap in electronic state distributions of Sc and C in the deep energy interval from –3 to –1 eV. Combined with the above analysis, it can be inferred that Sc forms stable bonds and interactions with the surrounding C. In addition, there are 3d electronic states of Sc distributed near the Fermi energy level, suggesting that Sc@C_{DV} has the potential to adsorb CO_2 and undergo subsequent catalytic process. As depicted in Fig. 1(d), the study employed the NVT ensemble for Sc@C_{DV} at 400 K in *ab initio* molecular dynamics (AIMD). The structures of Sc@C_{DV} at 0, 5 and 10 ps of the simulations are shown in Fig. 1(d). It can be seen that the structure as a whole remains stable. And the energy of the structure changes within 3 eV during 10 ps, which indicates that Sc@C_{DV} is thermally stable at room temperature.

2.2 Screening for TM@C

Given that the competing reaction for CO_2RR is the HER, a strong HER performance can detrimentally impact product selectivity[61]. Therefore, the study delved into the HER behaviors of TM@C, exemplified by Sc. Fig. 2(a) illustrates the structure of H^+ bound to the surface of Sc@C_{DV}, and Fig. 2(b) shows the energy change of the first step in the HER occurring in TM@C. Among them, the energy variations of Ti@C_{SV}, V@C_{SV}, V@C_{DV}, Cr@C_{SV}, Cr@C_{DV}, Mn@C_{SV}, Mn@C_{DV}, Fe@C_{SV}, Fe@C_{DV}, Co@C_{SV}, Co@C_{DV}, Ni@C_{SV} and Cu@C_{SV} are in the range from –0.5 to 0.5 eV, which indicate that they have good HER performance. In contrast, Sc@C_{SV},

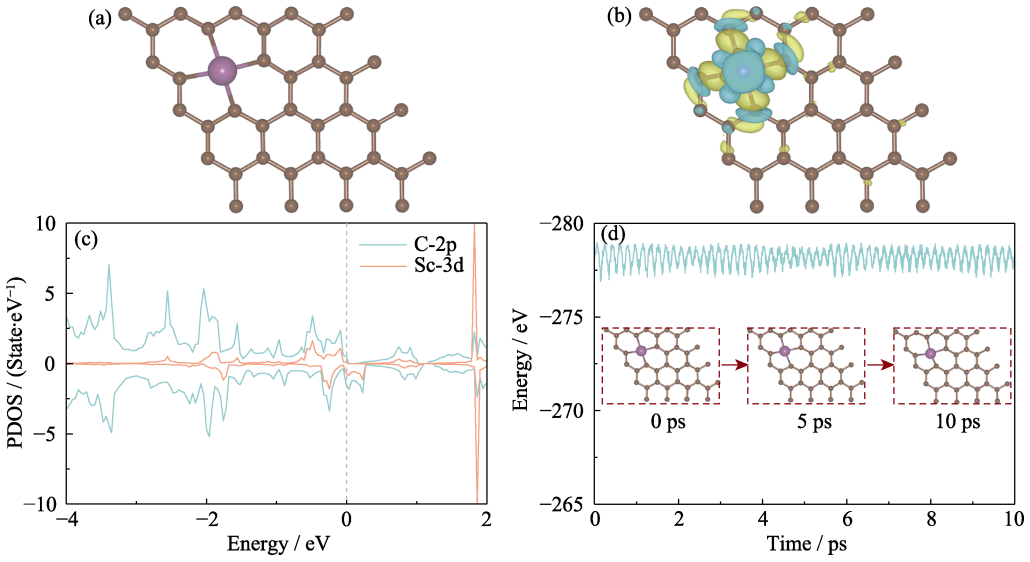

Fig. 1　Analyses for Sc@C_{DV}

(a) Structure of Sc@C_{DV}; (b) Charge density difference of Sc@C_{DV} with an isovalue of 0.005 e/Å^3 (positive and negative charges are shown in green and yellow); (c) PDOS diagram of Sc@C_{DV}; (d) AIMD simulations of Sc@C_{DV} (purple: Sc, brown: C); Colorful figures are available on website

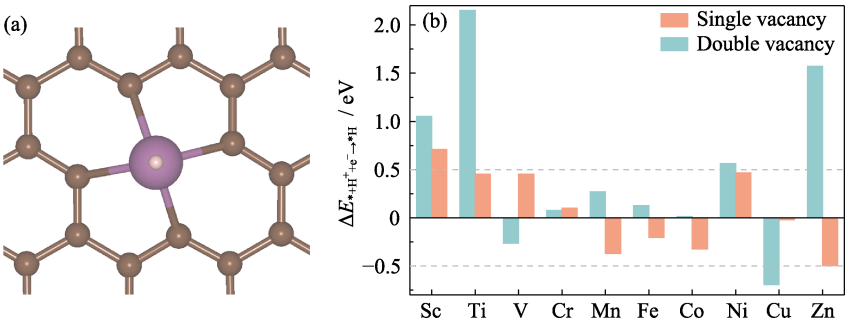

Fig. 2 Structure of H^+ adsorption on $Sc@C_{DV}$ (a) and energy changes of H^+ adsorption on TM@C (b)
Green in (a): H; Colorful figures are available on website

$Sc@C_{DV}$, $Ti@C_{DV}$, $Ni@C_{DV}$, $Cu@C_{DV}$, $Zn@C_{DV}$ and $Zn@C_{SV}$ exhibit relatively poor performance in HER, indicating better selectivity towards the CO_2RR. This phenomenon is crucial for maintaining high selectivity in CO_2RR.

The initial step in the CO_2 reduction process typically involves adsorption by the catalyst. Therefore, the study explored CO_2 adsorption on $TM@C_{SV}$ and $TM@C_{DV}$ surfaces, and their binding energies (E_b) are displayed in Fig. S4. Notably, $V@C_{DV}$, $Cr@C_{DV}$, $Mn@C_{DV}$, $Fe@C_{DV}$, $Cu@C_{DV}$, $Zn@C_{SV}$ and $Zn@C_{DV}$ spontaneously break down the adsorbed CO_2 into CO and adsorbed O atoms. It means that they adsorb CO_2 too strongly. The adsorbed O atoms from CO_2 decomposition can occupy the active sites, resulting in poisoning of the catalyst and inefficiency of CO_2RR process. Moreover $Co@C_{SV}$, $Co@C_{DV}$, $Ni@C_{SV}$ and $Ni@C_{DV}$ have positive energy changes for CO_2 adsorption, which indicates that they have difficulty in adsorbing CO_2. Especially, only $Sc@C_{SV}$, $Sc@C_{DV}$ and $Ti@C_{DV}$ exhibit thermodynamically favorable CO_2 adsorption behavior. In contrast, among the catalysts formed on single vacancy graphene substrates, all systems demonstrate the ability to adsorb the *HCOO or *COOH intermediates, which are usually produced in the first step of CO_2 reduction[62].

2.3 Activities of $Sc@C_{SV}$, $Sc@C_{DV}$ and $Ti@C_{DV}$

The study further explored the potentials of $Sc@C_{SV}$, $Sc@C_{DV}$ and $Ti@C_{DV}$ reducing CO_2 to CO and HCOOH. The energy change diagrams are shown in Fig. 3(a-c), and corresponding structures displayed in Fig. S5. The most thermodynamically probable pathway for $Sc@C_{SV}$, $Sc@C_{DV}$ and $Ti@C_{DV}$ involves *HCOO → *HCOOH → HCOOH + *, ultimately yielding the $2e^-$ product HCOOH. The rate-determining steps for $Sc@C_{DV}$ and $Ti@C_{DV}$ are *HCOO → *HCOOH and *HCOOH → HCOOH + *, corresponding to ΔG of 0.96 and 1.07 eV, respectively. In addition, the rate-determining step for $Sc@C_{SV}$ is the same as that for $Sc@C_{DV}$ (*HCOO → *HCOOH), but ΔG is 1.15 eV. Further, initial steps in the reduction of CO_2 by $Sc@C_{SV}$, $Sc@C_{DV}$ and $Ti@C_{DV}$, which is the formation of *HCOO, correspond to ΔG of 0.32, 0.29 and 0.41 eV, respectively. This implies that while the formation of *HCOO is thermodynamically favored over *COOH, the generation of *COOH is still feasible. The intermediate *COOH has the potential to generate both HCOOH and CO. The *COOH pathway exhibits similar behavior on $Sc@C_{SV}$ and $Sc@C_{DV}$, as shown in Fig. 3(a, b). *COOH → *HCOOH is the thermodynamically favorable process, while *COOH → H_2O + *CO is thermodynamically inhibited. The evidence suggests that *HCOOH is more likely to be the intermediate after *COOH is hydrogenated on $Sc@C_{SV}$ and $Sc@C_{DV}$. Both *COOH → H_2O + *CO and *COOH → *HCOOH processes carried out on $Ti@C_{DV}$ are thermodynamically favorable. Therefore $Sc@C_{SV}$ and $Sc@C_{DV}$ are anticipated to exhibit superior selectivity for HCOOH compared to $Ti@C_{DV}$.

Actually, $Sc@C_{SV}$, $Sc@C_{DV}$ and $Ti@C_{DV}$ exhibit selectivity for HCOOH, as evidenced by the comparison of energy changes during the first step of adsorption in their HER and CO_2RR processes (Fig. 3(d)). This indicates their capability to greatly inhibit HER. Both $Sc@C_{SV}$ and $Sc@C_{DV}$ can produce HCOOH *via* *HCOO → *HCOOH → HCOOH + * and *COOH → *HCOOH → HCOOH + * pathways, as illustrated in Fig. 3(a, b) and Fig. S5. For $Sc@C_{DV}$, the rate-determining step in *COOH → *HCOOH → HCOOH + * is the final HCOOH desorption, which is a process without electron transfer. Therefore, it is thermodynamically favorable with an energy change of less than 0.9 eV. The efficient reduction of CO_2 to HCOOH on $Sc@C_{DV}$ involves overcoming the ΔG of *HCOO → *HCOOH (0.96 eV) in the dominant pathway. In contrast, $Sc@C_{SV}$ forms *HCOO with a ΔG of 1.15 eV. In summary, $Sc@C_{DV}$ emerges as a highly promising catalyst for CO_2RR, demonstrating effective inhibition of the major competing reaction, HER, along with high selectivity for HCOOH and overall high efficiency.

2.4 Factors influencing the activity

The superior performance of $Sc@C_{DV}$ compared to $Sc@C_{SV}$ and $Ti@C_{DV}$ can be attributed to the effective

balance between the ΔG for hydrogenation of intermediate and the desorption difficulty. Among the three, Ti@C_{DV} exhibits the lowest ΔG of 0.62 eV for the hydrogenation of the intermediate *HCOO. This difference may be related to the number of electrons carried by the transition metal, with Ti having four valence electrons, one more than Sc. Bader charge analysis (Table S1 and Table S2) indicates that Ti retains 2.63|e| valence electrons after HCOO adsorption, while Sc, on the single and double vacancies, retains 1.68|e| and 1.50|e|, respectively. Clearly, Ti, with more electrons, is more prone to providing electrons for the coupling of protons during hydrogenation. The PDOS of Ti@C_{DV}, Sc@C_{SV} and Sc@C_{DV} are shown in Fig. 4(a-c),

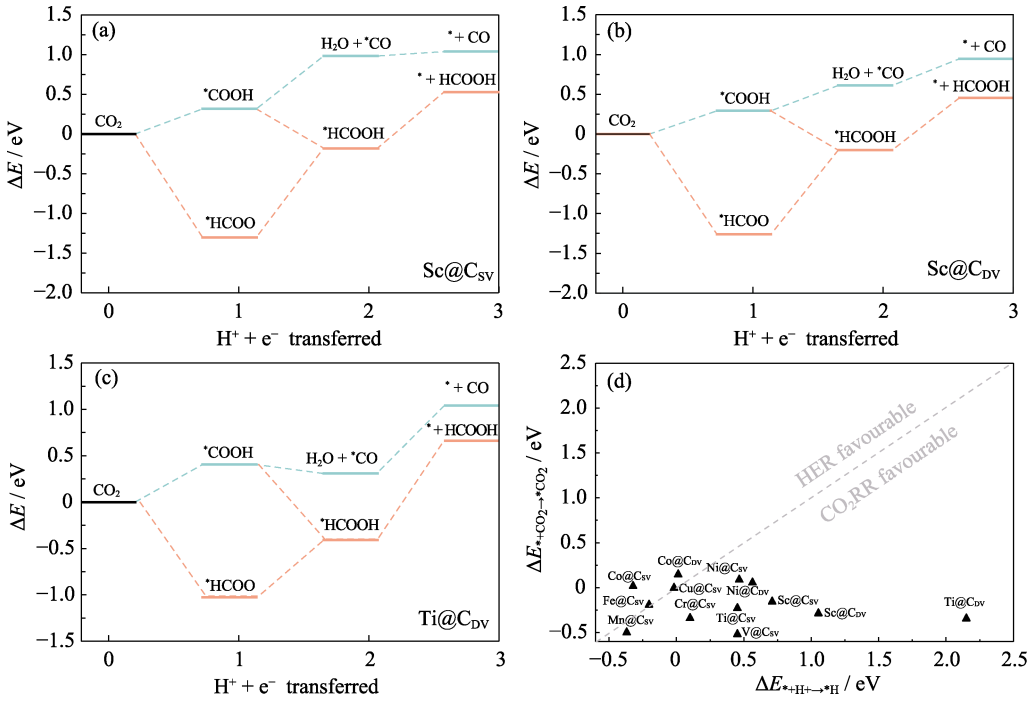

Fig. 3　Gibbs free energy profiles and the competitive reaction analysis

(a-c) Free energies of Sc@C_{SV} (a), Sc@C_{DV} (b) and Ti@C_{DV} (c); (d) CO_2RR *vs* HER for TM@C; Colorful figures are available on website

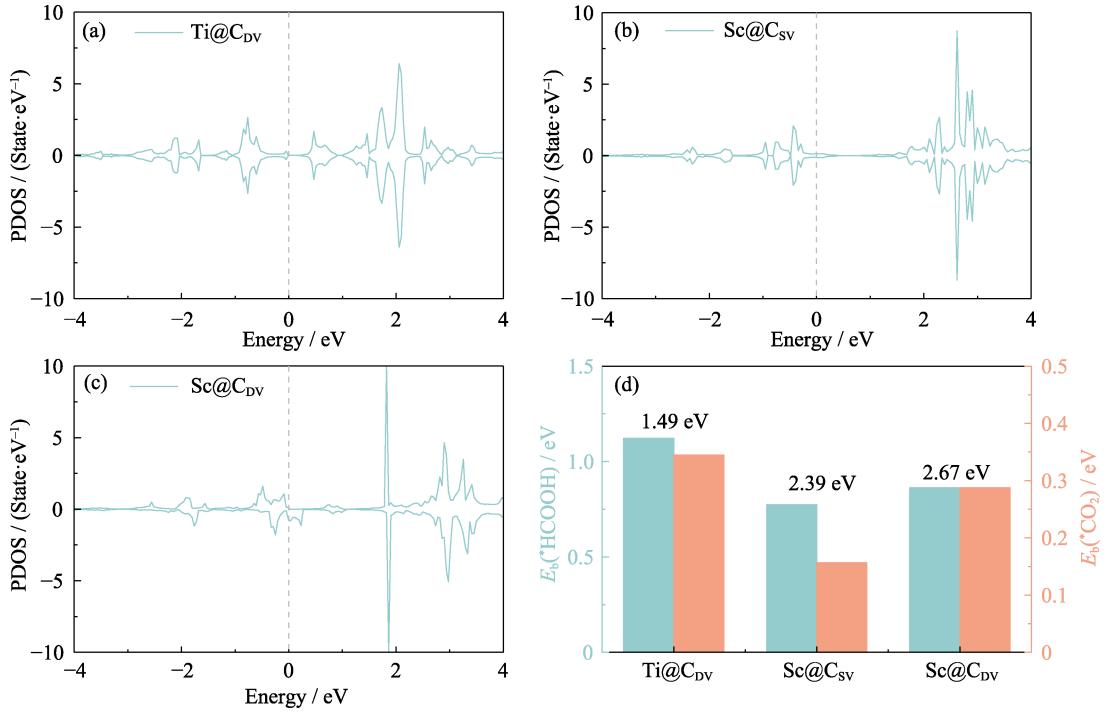

Fig. 4　Electron distributions of Ti@C_{DV}, Sc@C_{SV} and Sc@C_{DV}

(a-c) PDOS of Ti@C_{DV} (a), Sc@C_{SV} (b) and Sc@C_{DV} (c) (Gray dashed lines mark the positions of the Fermi energy levels); (d) E_b(*HCOOH) and E_b(*CO_2) of Ti@C_{DV}, Sc@C_{SV} and Sc@C_{DV}; The d-band center as an average of the d-band energies; Colorful figures are available on website

As discussed earlier, Ti@C_{DV} has more active electronic states distributed near the Fermi energy level, which is favorable for reduction of CO_2. This is further illustrated by the d-band centers shown in Fig. 4(d), where the d-band centers of Ti@C_{DV}, Sc@C_{SV} and Sc@C_{DV} are 1.49, 2.39 and 2.67 eV, respectively. The d-band center as an average of the d-band energies, well describes the distribution of electrons in the d state of the metal[63]. A closer proximity of the d-band center to the Fermi energy level usually signifies a stronger attraction to small molecules[64-66]. Ti, due to its more valence electrons, although more conducive to hydrogenation, also encounters challenges in desorption. A distinction also arises between Sc@C_{SV} and Sc@C_{DV} due to the difference in substrate. Binding Sc on graphene with double vacancies can provide more reactive electrons compared to graphene with single vacancies, rendering Sc@C_{DV} more advantageous than Sc@C_{SV} during the hydrogenation reaction. In conclusion, the superior performance of Sc@C_{DV} roots in the effective balance between the ΔG of hydrogenation and desorption.

3 Conclusions

This study systematically explored the potential of 3d transition metal single-atom catalysts on graphene vacancies for CO_2RR. Combined with the ability to inhibit HER and adsorb CO_2, there were 20 possible TM@C catalysts screened and Sc@C_{SV}, Sc@C_{DV} and Ti@C_{DV} were identified to have the most potential. Thermal stability of Sc@C_{DV} at room temperature was also demonstrated by AIMD. In the study of the CO_2 reduction process, Sc@C_{SV}, Sc@C_{DV} and Ti@C_{DV} exhibited superior selectivity for HCOOH, and Sc@C_{DV} requires only 0.96 eV of ΔG to effectively reduce CO_2 to HCOOH. Notably, three catalysts above all effectively inhibit HER during CO_2RR. The enhanced performance of Sc@C_{DV} is attributed to a balance between ΔG of hydrogenation and product desorption.

Supporting materials

Supporting materials related to this article can be found at https://doi.org/10.15541/jim20230549.

References:

[1] FENG Q, LIU D, ZHANG Y, *et al.* Thermodynamic and first-principles assessments of materials for solar-driven CO_2 splitting using two-step thermochemical cycles. *Journal of Inorganic Materials*, 2022, **37(2):** 223.

[2] TIAN J, MA X, WANG M, *et al.* Sn quantum dots for electrocatalytic reduction of CO_2 to HCOOH. *Journal of Inorganic Materials*, 2021, **36(12):** 1337.

[3] CHEN S, LÜ G. CO_2 methanation over Ru/TiO_2 catalysts under UV irradiation and heating. *Journal of Inorganic Materials*, 2014, **29(12):** 1287.

[4] MIKKELSEN M, JØRGENSEN M, KREBS F C. The teraton challenge. a review of fixation and transformation of carbon dioxide. *Energy & Environmental Science*, 2010, **3(1):** 43.

[5] XU X, GOU X, ZHANG W, *et al.* A bibliometric analysis of carbon neutrality: research hotspots and future directions. *Heliyon*, 2023, **9(8):** e18763.

[6] HUA Y, WANG J, MIN T, *et al.* Electrochemical CO_2 conversion towards syngas: recent catalysts and improving strategies for ratio-tunable syngas. *Journal of Power Sources*, 2022, **535:** 231453.

[7] HE R, XU N, HASAN I M U, *et al.* Advances in electrolyzer design and development for electrochemical CO_2 reduction. *EcoMat*, 2023, **5(7):** e12346.

[8] KOUA K A J, PENG J, ZHANG P, *et al.* Unveiling the magnetic ordering effect in La-doped $Ti_3C_2O_2$ MXenes on electrocatalytic CO_2 reduction. *Journal of Materials Chemistry A*, 2024, **12(1):** 303.

[9] ROY S C, VARGHESE O K, PAULOSE M, *et al.* Toward solar fuels: photocatalytic conversion of carbon dioxide to hydrocarbons. *ACS Nano*, 2010, **4(3):** 1259.

[10] ZHANG W, JIN Z, CHEN Z. Rational-designed principles for electrochemical and photoelectrochemical upgrading of CO_2 to value-added chemicals. *Advanced Science*, 2022, **9(9):** 2105204.

[11] LI N, LIU J, DONG B X, *et al.* Polyoxometalate-based compounds for photo-and electrocatalytic applications. *Angewandte Chemie International Edition*, 2020, **59(47):** 20779.

[12] WU Q J, LIANG J, HUANG Y B, *et al.* Thermo-, electro-, and photocatalytic CO_2 conversion to value-added products over porous metal/covalent organic frameworks. *Accounts of Chemical Research*, 2022, **55(20):** 2978.

[13] NIE X, ESOPI M R, JANIK M J, *et al.* Selectivity of CO_2 reduction on copper electrodes: the role of the kinetics of elementary steps. *Angewandte Chemie International Edition*, 2013, **125(9):** 2519.

[14] JIA Y, ZHANG L, DU A, *et al.* Defect graphene as a trifunctional catalyst for electrochemical reactions. *Advanced Materials*, 2016, **28(43):** 9532.

[15] XUE Z H, ZHANG S N, LIN Y X, *et al.* Electrochemical reduction of N_2 into NH_3 by donor-acceptor couples of Ni and Au nanoparticles with a 67.8% Faradaic efficiency. *Journal of the American Chemical Society*, 2019, **141(38):** 14976.

[16] JONES J P, PRAKASH G K S, OLAH G A. Electrochemical CO_2 reduction: recent advances and current trends. *Israel Journal of Chemistry*, 2014, **54(10):** 1451.

[17] ZHAO K, QUAN X. Carbon-based materials for electrochemical reduction of CO_2 to C^{2+} oxygenates: recent progress and remaining challenges. *ACS Catalysis*, 2021, **11(4):** 2076.

[18] DENG J, IÑIGUEZ J A, LIU C. Electrocatalytic nitrogen reduction at low temperature. *Joule*, 2018, **2(5):** 846.

[19] AZOFRA L M, LI N, MACFARLANE D R, *et al.* Promising prospects for 2D d^2–d^4 M_3C_2 transition metal carbides (MXenes) in N_2 capture and conversion into ammonia. *Energy & Environmental Science*, 2016, **9(8):** 2545.

[20] LI B, WU Y, LI N, *et al.* Single-metal atoms supported on MBenes for robust electrochemical hydrogen evolution. *ACS Applied Materials & Interfaces*, 2020, **12(8):** 9261.

[21] FU Y, BI M, LI C, *et al.* Research progress on non-noble metal/nitrogen-doped carbon composite materials in electrocatalytic oxygen evolution reaction. *Journal of Inorganic Materials*, 2022, **37(2):** 163.

[22] LI Z, SUN Q, CHEN S, *et al.* Hydrothermal synthesized nickel copper composite phosphides as bifunctional electrocatalysts for hydrogen evolution and hydrazine oxidation. *Journal of Inorganic Materials*, 2020, **35(10):** 1149.

[23] FRANCKE R, SCHILLE B, ROEMELT M. Homogeneously catalyzed electroreduction of carbon dioxide-methods, mechanisms, and catalysts. *Chemical Reviews*, 2018, **118(9):** 4631.

[24] TODOROVA T K, SCHREIBER M W, FONTECAVE M. Mechanistic understanding of CO_2 reduction reaction (CO_2RR) toward multicarbon products by heterogeneous copper-based catalysts. *ACS Catalysis*, 2020, **10(3):** 1754.

[25] WANG G, CHEN J, DING Y, *et al.* Electrocatalysis for CO_2 conversion: from fundamentals to value-added products. *Chemical Society Reviews*, 2021, **50(8):** 4993.

[26] MA W, HE X, WANG W, *et al.* Electrocatalytic reduction of CO_2 and CO to multi-carbon compounds over Cu-based catalysts. *Chemical Society Reviews*, 2021, **50(23):** 12897.

[27] PENG J, SHI Z, JIANG J, *et al.* Charge-orbital synergistic engineering of TM@ $Ti_3C_2O_{1-x}B_x$ for highly selective CO_2 electrochemical reduction. *Materials Horizons*, 2023, **10(10):** 4278.

[28] QIAO B, LIU J, ALLARD L, *et al.* Single-atom catalysis: Pt_1/FeO_x for CO oxidation and preferential oxidation of CO in H_2. *Microscopy and Microanalysis*, 2012, **18(S2):** 350.

[29] WANG X, ZHANG Y, WU J, *et al.* Single-atom engineering to ignite 2D transition metal dichalcogenide based catalysis: fundamentals, progress, and beyond. *Chemical Reviews*, 2022, **122(1):** 1273.

[30] CHENG N, ZHANG L, DOYLE-DAVIS K, *et al.* Single-atom catalysts: from design to application. *Electrochemical Energy Reviews*, 2019, **2(4):** 539.

[31] LI M, WANG H, LUO W, *et al.* Heterogeneous single-atom catalysts for electrochemical CO_2 reduction reaction. *Advanced Materials*, 2020, **32(34):** 2001848.

[32] QU G, WEI K, PAN K, *et al.* Emerging materials for electrochemical CO_2 reduction: progress and optimization strategies of carbon-based single-atom catalysts. *Nanoscale*, 2023, **15(8):** 3666.

[33] WANG Y, LIU Y, LIU W, *et al.* Regulating the coordination structure of metal single atoms for efficient electrocatalytic CO_2 reduction. *Energy & Environmental Science*, 2020, **13(12):** 4609.

[34] CHEN X, ZHAO X, KONG Z, *et al.* Unravelling the electrochemical mechanisms for nitrogen fixation on single transition metal atoms embedded in defective graphitic carbon nitride. *Journal of Materials Chemistry A*, 2018, **6(44):** 21941.

[35] HUANG B, LI N, ONG W J, *et al.* Single atom-supported MXene: how single-atomic-site catalysts tune the high activity and selectivity of electrochemical nitrogen fixation. *Journal of Materials Chemistry A*, 2019, **7(48):** 27620.

[36] YAO M, SHI Z, ZHANG P, *et al.* Density functional theory study of single metal atoms embedded into MBene for electrocatalytic conversion of N_2 to NH_3. *ACS Applied Nano Materials*, 2020, **3(10):** 9870.

[37] DU Z, CHEN X, HU W, *et al.* Cobalt in nitrogen-doped graphene as single-atom catalyst for high-sulfur content lithium-sulfur batteries. *Journal of the American Chemical Society*, 2019, **141(9):** 3977.

[38] GU J, HSU C S, BAI L, *et al.* Atomically dispersed Fe^{3+} sites catalyze efficient CO_2 electroreduction to CO. *Science*, 2019, **364(6445):** 1091.

[39] ZHANG Z, ZHU J, CHEN S, *et al.* Liquid fluxional Ga single atom catalysts for efficient electrochemical CO_2 reduction. *Angewandte Chemie International Edition*, 2023, **62(3):** e202215136.

[40] HAN S S, LIU L Y, SHAN Y K, *et al.* Research of graphene/antireflection nanostructure composite transparent conducting films. *Journal of Inorganic Materials*, 2017, **32(2):** 197.

[41] WANG Y, LI S, YANG H, *et al.* Progress in the functional modification of graphene/graphene oxide: a review. *RSC Advances*, 2020, **10(26):** 15328.

[42] WANG J, JIN X, LI C, *et al.* Graphene and graphene derivatives toughening polymers: toward high toughness and strength. *Chemical Engineering Journal*, 2019, **370:** 831.

[43] HE J L, SONG E H, WANG L J, *et al.* DFT Calculation of NO adsorption on Cr doped graphene. *Journal of Inorganic Materials*, 2021, **36(10):** 1047.

[44] XING W W, ZHANG C X, FAN S C, *et al.* Research progress on resonant characteristics of graphene. *Journal of Inorganic Materials*, 2016, **31(7):** 673.

[45] NAN H, WANG W L, HAN J H, *et al.* Low-cost preparation of graphene papers from chemical reduction with FeI_2/Ni^{2+} for conductivity and catalytic property. *Journal of Inorganic Materials*, 2017, **32(9):** 997.

[46] CHOI J H, LEE J, BYEON M, *et al.* Graphene-based gas sensors with high sensitivity and minimal sensor-to-sensor variation. *ACS Applied Nano Materials*, 2020, **3(3):** 2257.

[47] GATTRELL M, GUPTA N, CO A. A review of the aqueous electrochemical reduction of CO_2 to hydrocarbons at copper. *Journal of Electroanalytical Chemistry*, 2006, **594(1):** 1.

[48] LI C W, KANAN M W. CO_2 reduction at low overpotential on Cu electrodes resulting from the reduction of thick Cu_2O films. *Journal of the American Chemical Society*, 2012, **134(17):** 7231.

[49] SCHOUTEN K J P, PÉREZ GALLENT E, KOPER M T. Structure sensitivity of the electrochemical reduction of carbon monoxide on copper single crystals. *ACS Catalysis*, 2013, **3(6):** 1292.

[50] REN D, DENG Y, HANDOKO A D, *et al.* Selective electrochemical reduction of carbon dioxide to ethylene and ethanol on copper (I) oxide catalysts. *ACS Catalysis*, 2015, **5(5):** 2814.

[51] RESKE R, MISTRY H, BEHAFARID F, *et al.* Particle size effects in the catalytic electroreduction of CO_2 on Cu nanoparticles. *Journal of the American Chemical Society*, 2014, **136(19):** 6978.

[52] JIAO L, YANG W, WAN G, *et al.* Single-atom electrocatalysts from multivariate metal-organic frameworks for highly selective reduction of CO_2 at low pressures. *Angewandte Chemie International Edition*, 2020, **59(46):** 20589.

[53] KRESSE G, FURTHMÜLLER J. Efficiency of *ab-initio* total energy calculations for metals and semiconductors using a plane-wave basis set. *Computational Materials Science*, 1996, **6(1):** 15.

[54] KRESSE G, FURTHMÜLLER J. Efficient iterative schemes for *ab initio* total-energy calculations using a plane-wave basis set. *Physical Review B*, 1996, **54(16):** 11169.

[55] PERDEW J P, BURKE K, ERNZERHOF M. Generalized gradient approximation made simple. *Physical Review Letters*, 1996, **77(18):** 3865.

[56] KRESSE G, JOUBERT D. From ultrasoft pseudopotentials to the projector augmented-wave method. *Physical Review B*, 1999, **59(3):** 1758.

[57] BLÖCHL P E. Projector augmented-wave method. *Physical Review B*, 1994, **50(24):** 17953.

[58] GRIMME S. Semiempirical GGA-type density functional constructed with a long-range dispersion correction. *Journal of Computational Chemistry*, 2006, **27(15):** 1787.

[59] SKÚLASON E, BLIGAARD T, GUDMUNDSDÓTTIR S, *et al.* A theoretical evaluation of possible transition metal electro-catalysts for N_2 reduction. *Physical Chemistry Chemical Physics*, 2012, **14(3):** 1235.

[60] LI J, XU J, ZHAO J, *et al.* Modulation of oxygen-etching for generating nickel single atoms for efficient electroreduction of CO_2

to syngas (CO/H_2). *Journal of Catalysis*, 2023, **421:** 332.

[61] LI N, WANG X, LU X, *et al.* Comprehensive mechanism of CO_2 electroreduction on non-noble metal single-atom catalysts of Mo_2CS_2-MXene. *Chemistry–A European Journal*, 2021, **27(71):** 17900.

[62] LI N, CHEN X, ONG W J, *et al.* Understanding of electrochemical mechanisms for CO_2 capture and conversion into hydrocarbon fuels in transition-metal carbides (MXenes). *ACS Nano*, 2017, **11(11):** 10825.

[63] JIAO S, FU X, HUANG H. Descriptors for the evaluation of electrocatalytic reactions: d-band theory and beyond. *Advanced Functional Materials*, 2022, **32(4):** 2107651.

[64] NØRSKOV J K, BLIGAARD T, LOGADOTTIR A, *et al.* Trends in the exchange current for hydrogen evolution. *Journal of The Electrochemical Society*, 2005, **152(3):** J23.

[65] NØRSKOV J K, ABILD-PEDERSEN F, STUDT F, *et al.* Density functional theory in surface chemistry and catalysis. *Proceedings of the National Academy of Sciences*, 2011, **108(3):** 937.

[66] KITCHIN J R, NØRSKOV J K, BARTEAU M A, *et al.* Role of strain and ligand effects in the modification of the electronic and chemical properties of bimetallic surfaces. *Physical Review Letters*, 2004, **93(15):** 156801.

3d 过渡金属单原子掺杂石墨烯缺陷电催化还原 CO_2 的第一性原理研究

靳宇翔[1], 宋二红[2], 朱永福[1]

(1. 吉林大学 材料科学与工程学院, 长春 130025; 2. 中国科学院 上海硅酸盐研究所, 上海 200050)

摘 要: 将 CO_2 高效转化为有价值的化学品(如 CO 和 HCOOH 等)是缓解环境问题、实现碳中和的重要措施。然而 CO_2 还原反应(CO_2RR)有着产物多样和路径复杂的特点, 再加上目前难以确定影响 CO_2RR 活性的真正因素, 使得设计对特定产物有高选择性和高活性的催化剂十分具有挑战性。本研究从第一性原理出发, 系统研究了 3d 过渡金属单原子掺杂石墨烯单个空位($TM@C_{SV}$)和双空位($TM@C_{DV}$)电催化还原 CO_2 的潜力, 具体涵盖基底的稳定性、中间产物热力学吸附以及与之竞争的析氢反应(HER)。通过对 Sc, Ti, V, Cr, Mn, Fe, Co, Ni, Cu 和 Zn 掺杂石墨烯缺陷后形成的 20 种催化剂进行筛选, 发现 Sc 原子掺杂石墨烯单个空位的 $Sc@C_{SV}$ 和 Sc、Ti 原子掺杂石墨烯双空位的 $Sc@C_{DV}$ 和 $Ti@C_{DV}$ 同时具备吸附 CO_2 分子和抑制 HER 的能力。其中 $Sc@C_{DV}$ 对 HCOOH 表现出最佳的活性和选择性, 速率决定步骤的吉布斯自由能差仅为 0.96 eV。最后, 通过电子结构分析进一步揭示了 $Sc@C_{DV}$ 优于其他催化剂的原因是 $Sc@C_{DV}$ 调整了费米能级附近的活性电子态, 从而实现对 CO_2 的高效还原。

关 键 词: 第一性原理; 单原子催化剂; CO_2 还原反应; HCOOH; 碳中和

中图分类号: TQ174 **文献标志码:** A **文章编号:** 1000-324X(2024)07-0845-08

Supporting Materials:

First-principles Investigation of Single 3d Transition Metals Doping Graphene Vacancies for CO_2 Electroreduction

JIN Yuxiang[1], SONG Erhong[2], ZHU Yongfu[1]

(1. School of Materials Science and Engineering, Jilin University, Changchun 130025, China; 2. Shanghai Institute of Ceramics, Chinese Academy of Sciences, Shanghai 200050, China)

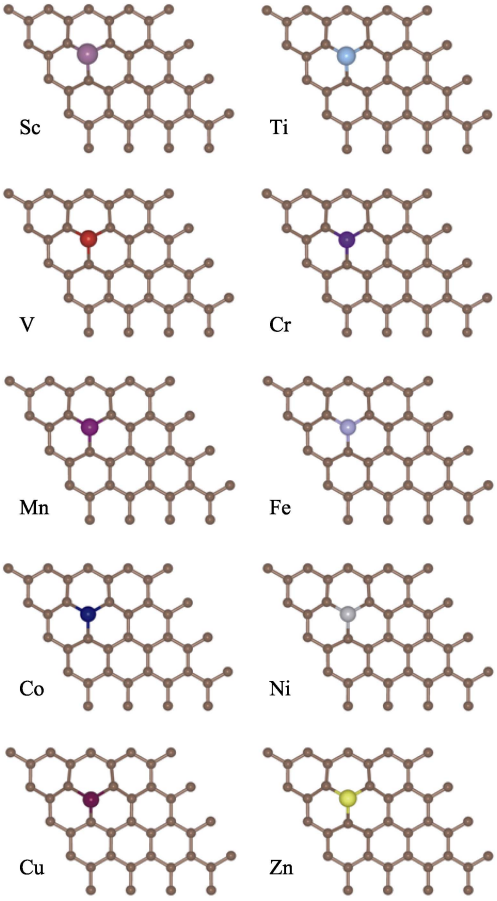

Fig. S1　Structures of TM@C_{SV} (TM = Sc, Ti, V, Cr, Mn, Fe, Co, Ni, Cu and Zn)

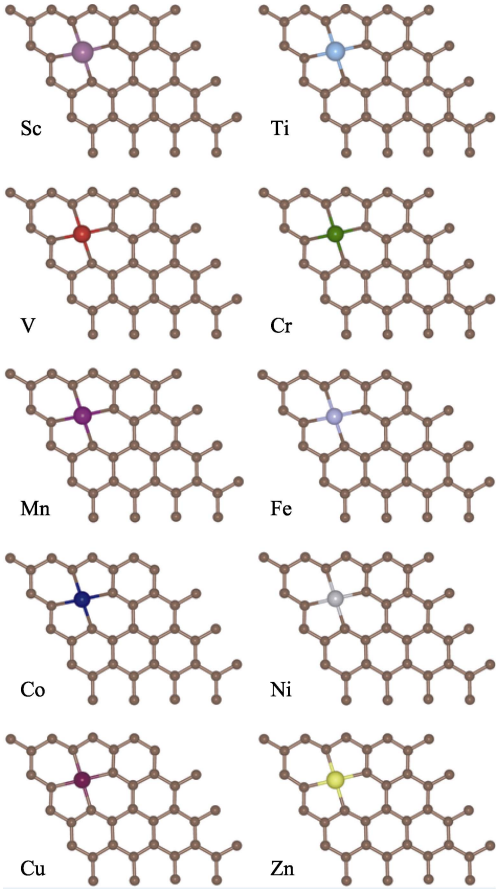

Fig. S2　Structures of TM@C_{DV} (TM = Sc, Ti, V, Cr, Mn, Fe, Co, Ni, Cu and Zn)

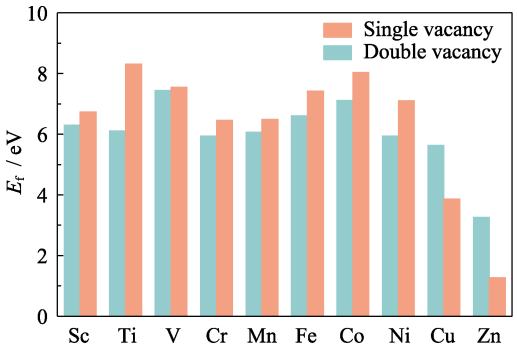

Fig. S3　Formation energies of TM at graphene single and double vacancies

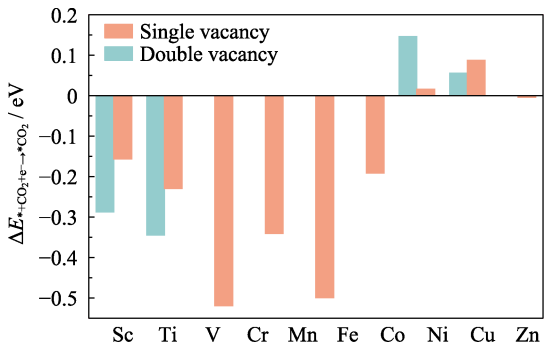

Fig. S4　Binding energies of adsorption CO_2 on TM@C_{SV} and TM@C_{DV}

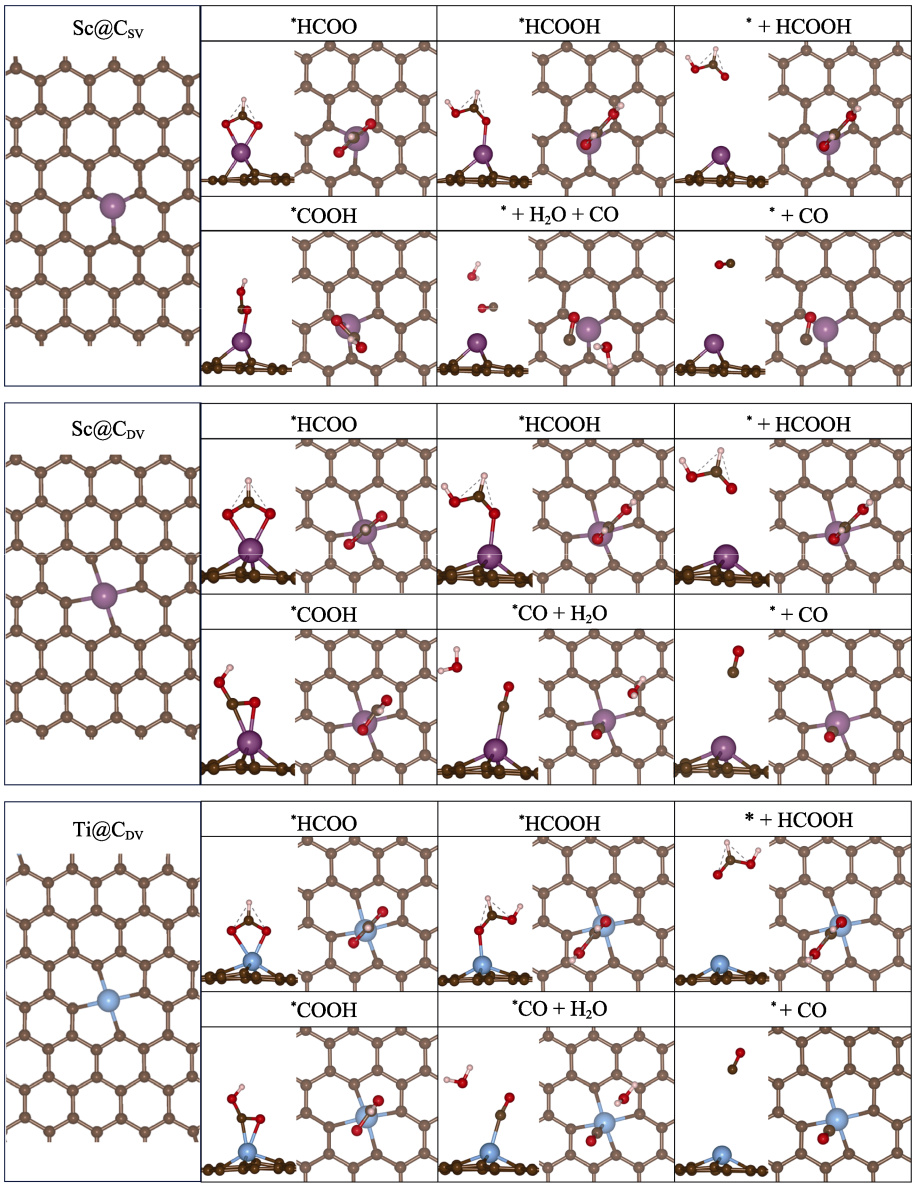

Fig. S5 Intermediate structures of Sc@C_{SV}, Sc@C_{DV} and Ti@C_{DV} in the CO_2RR

Table S1 Max lengthes of TM–C and Bader charges of TM for TM@C_{SV}

TM@C_{SV}	Max length of TM-C/Å	Bader charge/|e|
Sc@C_{SV}	2.08	+1.50
Ti@C_{SV}	1.94	+1.37
V@C_{SV}	1.89	+1.22
Cr@C_{SV}	1.86	+1.35
Mn@C_{SV}	1.83	+1.00
Fe@C_{SV}	1.76	+0.67
Co@C_{SV}	1.76	+0.72
Ni@C_{SV}	1.79	+0.63
Cu@C_{SV}	1.89	+0.02
Zn@C_{SV}	1.96	+0.76

Table S2　Max lengthes of TM–C and Bader charges of TM for TM@C_{DV}

TM@C_{DV}	Max length of TM–C/Å	Bader charge/|e|
Sc@C_{DV}	2.24	+1.32
Ti@C_{DV}	2.07	+0.94
V@C_{DV}	2.02	+1.22
Cr@C_{DV}	2.01	+0.93
Mn@C_{DV}	1.99	+0.64
Fe@C_{DV}	1.97	+0.61
Co@C_{DV}	1.95	+0.34
Ni@C_{DV}	1.91	+0.18
Cu@C_{DV}	1.90	+0.18
Zn@C_{DV}	1.93	+0.10